Acta Cryst. (1999). B**55**, 923–930

Electron density and electrostatic potential of $KNiF_3$: multipole, orbital and topological analyses of vacuum-camera-imaging plate and four-circle diffractometer data

Yury Ivanov,[a] Elizabeth A. Zhurova,[b]† Vladimir V. Zhurov,[c] Kiyoaki Tanaka[b] and Vladimir Tsirelson[a]*

[a]*Mendeleev University of Chemical Technology, Moscow 125047, Russia,* [b]*CREST, Japanese Science and Technology Corporation, Nagoya Institute of Technology, Gokiso-cho, Showa-ku, Nagoya 466, Japan, and* [c]*Karpov Institute of Physical Chemistry, ul. Vorontsovo pole 10, 103064 Moscow, Russia. E-mail: tsirel@muctr.edu.ru*

(*Received 13 April 1999; accepted 5 July 1999*)

Abstract

The electron density and electrostatic potential of $KNiF_3$, nickel potassium trifluoride, were studied using multipole and orbital model treatment of the precision X-ray diffraction data measured by vacuum-camera-imaging plate and four-circle diffractometer methods. Different experimental methods lead to similar multipole and atomic displacement parameters and to qualitatively the same electron densities. Good agreement was also achieved for the Laplacians of the electron density and the electrostatic potentials. Some pitfalls of the vacuum-camera-imaging plate method that could be improved are discussed.

1. Introduction

High-energy synchrotron radiation with short wavelengths, CCD detectors and imaging plates are becoming popular in accurate diffraction studies (Bolotovsky *et al.*, 1995; Graafsma *et al.*, 1997; Martin & Pinkerton, 1998). In this paper we will present the results of a high-resolution study of electron density (ED) in $KNiF_3$ cubic perovskite using diffraction data measured by the vacuum-camera-imaging plate method on a diffractometer with a molybdenum rotating anode X-ray source (VCIP experiment). This method combines, in principle, the advantages of all the methods mentioned above, avoiding the expense of synchrotron radiation (the latter, of course, provides the shorter radiation wavelengths). To estimate the potential of the VCIP method in practice an accurate X-ray experiment with a four-circle scintillation counter diffractometer was also performed (4C experiment). To compare the results obtained with different techniques we performed a multipole and orbital electron population, and topological analyses of both sets of structure factors.

Cubic perovskites contain one ABC_3 formula in the unit cell. The symmetry of the Ni- and K-atom positions is *m*3*m*, while the F atom is sited in the 4/*mmm* position. In an attempt to understand more the interesting physical properties, the ED of cubic perovskites was studied many times in terms of the difference Fourier maps (Kijima *et al.*, 1981; Kijima *et al.*, 1983; Miyata *et al.*, 1983; Buttner & Maslen, 1988; Maslen & Spadaccini, 1989; Zhurova *et al.*, 1995, Abramov *et al.*, 1995). The quantitative ED analysis has not been undertaken before, to our knowledge.

2. Experimental

The same spherical specimen with diameter 68 (2) μm, obtained by the flux method, was used in both experiments. The measurements were performed at room temperature. The cylindrical vacuum camera with diameter 110 mm and height 90 mm was mounted on the Mac Science diffractometer equipped with a molybdenum rotating anode X-ray source [V = 50 kV, I = 80 mA (VCIP) and 90 mA (4C)] and graphite monochromator (Tanaka *et al.*, 1999). Measurements were performed in the total range $0 < \varphi < 186°$, with each oscillation photograph being taken in 16° areas with 6° overlapping. Owing to imaging plate saturation, two different sets of measurements with exposure times 8 min and 2 h have been obtained in order to obtain a reasonable statistical precision for both the strong and weak reflections. Evacuation of the camera up to 70 mTorr allowed reduction of the average background level 50 times: the latter was ∼1–3 impulses for 8 min images and 20–30 impulses for 2 h ones.

The imaging plate was digitized using the Fuji BAS-2500 scanner with 50 × 50 μm pixel resolution. After indexing the reflections using the *DENZO* program (Otwinowski & Minor, 1997), the net integrated intensities were determined using the program *VIIPP* (Zhurov, 1998). The integration accounted for the $A + B\mathrm{tg}\theta$ angle dependence of the $\alpha_1 - \alpha_2$ splitting and orientation of the elliptical integration area along the direction of the increasing $\sin\theta/\lambda$. Lorentz and polarization corrections, as well as the corrections for the oblique incidence of the X-ray beam (Tanaka *et al.*, 1999) on the imaging plate, were applied. The total time of the VCIP intensity measurements was 72 working

† Permanent address: Institute of Crystallography, Russian Academy of Sciences, Leninsky Pr. 59, 117333 Moscow, Russia.

Table 1. *Crystallographic data, experimental and selected refinement information for $KNiF_3$*

Space group	*Pm3m*	
Cell dimensions (Å)	a = 4.0108 (1)	
Cell volume (Å^3)	64.5208	
$F(000)$	74	
Number of atoms in cell	3	
Linear absorption coefficient μ (cm^{-1})	89.8	
Sample radius (μm)	34 (1)	
Radiation and wavelength	Graphite-filtered Mo $K\alpha$, λ = 0.71069 Å	
Diffractometer	Mac Science with rotated Mo anode X-ray source	
	Vacuum camera	Four-circle plate
	Imaging plate method	Geometry
Mode of refinement	$F(hkl)$	$F(hkl)$
$(\sin\theta/\lambda)_{max}$ (Å^{-1})	1.35	1.34
Weighting scheme	$[\sigma^2(F_{obs}) + (0.0015F_{obs})^2]^{-1}$	$[\sigma^2(F_{obs}) + (0.008F_{obs})^2]^{-1}$
Extinction formalism	Becker & Coppens (1974)	
	Lorentz mosaic spread, type I	
Extinction parameter, $g \times 10^4$	0.0285 (26)	0.0292 (7)
Number of measured reflections	2719	1328
Number of independent reflections	144	166
$R_{int} = \Sigma(I_m - I_j)/\Sigma I_j$	0.0311	0.0245

hours. Other details of the VCIP data treatment procedure are described by Zhurova *et al.* (1999).

The standard procedure was used for the four-circle scintillation counter measurements (Tsirelson & Ozerov, 1996). Intensities of reflections were measured in the $\omega/2\theta$ scan mode with a speed of 2° min^{-1} on the same diffractometer. The scan range was changed according to 1.2 + 0.5tan θ (°). The stability of the intensity, controlled by measurement of reflections 200, 020 and 002 after every 30 reflections, was ±0.5%. The measurements were repeated to provide the statistical precision of 0.5%. Multiple diffraction was avoided using the ψ-scan method (Tanaka *et al.*, 1994). Only one reflection of the whole reciprocal space sphere with $2\theta < 30°$ was recognized as highly affected by multiple diffraction and removed. The reflections with $30 < 2\theta < 150°$ were mainly measured within one octant of the reciprocal space: some reflections were measured in other octants when multiple diffraction cannot be avoided. The lattice constant was determined over 25 high-angle reflections. Corrections for Lorentz and polarization factors and absorption were applied.

Both sets of intensities were corrected for absorption and thermal diffuse scattering (TDS) in a two-phonon approximation (Tsarkov & Tsirelson, 1991) using elastic constants from Hellwege (1979). Maximal TDS correction reached 15.4% for the $10,\bar{3}2$ reflection.

Experimental details are given in Table 1.

3. Refinements

3.1. *The multipole model*

The structural model used for the treatment of the experimental data is as follows. The ED was approximated using the multipole model of Hansen & Coppens (1978) and the anharmonicity of the atomic displacements was modeled using a Gram–Charlier expansion of the probability density function for atomic displacements up to tensors of fourth rank (*International Tables for Crystallography*, 1995). Preliminary harmonic refinements of a spherical atom model were carried out using high-angle data ($\sin\theta/\lambda \geq 0.75$ Å^{-1}). The atomic displacement parameters derived were taken as initial ones for further refinement.

The ED is approximated in the Hansen & Coppens (1978) multipole model as the sum of the pseudo-atomic electron densities in the form

$$\rho_{atomic}(\mathbf{r}) = \rho_{core}(r) + P_v\kappa'^3\rho_{valence}(\kappa' r) + \sum_{l=1}^{4}\kappa''^3 R_l(\kappa'' r)\sum_{m=-1}^{l} P_{lm}y_{lm}(\mathbf{r}/r).$$

The optimized parameters include the scale factor, the atomic valence-shell contraction–expansion parameters κ' and κ'', and the multipole populations P_v and P_{lm} up to the hexadecapole level ($l_{max} = 4$). Isotropic secondary

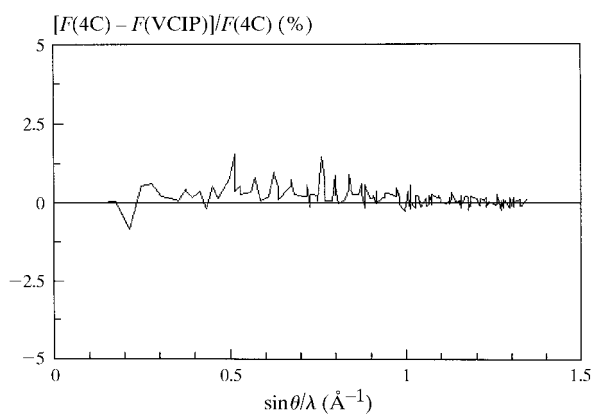

Fig. 1. Relative difference (%) between structure factors $[F(4C) - F(VCIP)]/F(4C)$. See text for explanation of the abbreviations.

extinction was described according to Becker & Coppens (1974). The exponential-type radial functions $r^{n_l}\exp(-\kappa'\xi r)$ with $n_2 = 2$, $n_4 = 4$ (F) and $n_4 = 8$ (K, Ni; Hansen & Coppens, 1978) and values of the orbital exponents $\xi_K = 6.0$, $\xi_{Ni} = 8.36$ and $\xi_F = 4.9$ a.u. were used. Anomalous dispersion corrections were taken from *International Tables for Crystallography* (1995). The unit-cell electroneutrality condition was imposed during the multipole refinement. Refinements were carried out using the *MOLDOS*97 program (Protas, 1995), based on the program *MOLLY* (Hansen & Coppens, 1978) modified for IBM PC.

The procedure of the multipole refinement based on $|F|$ was the same for both experiments. First, the scale factor, the extinction parameter, the electron density parameters κ', P_v and P_{lm}, and harmonic atomic displacement parameters were refined with all reflections (the weighting schemes are specified in Table 1). The lowest R factor was obtained when K was approximated by the ionic scattering function $P_v^K = 0$. Then the harmonic and anharmonic displacement parameters were refined using reflections with $\sin\theta/\lambda \geq 0.75$ Å^{-1} and then fixed. We recognized that the anharmonic parameters of the K atom are very small and are within the noise for both sets of data, therefore, displacement of this atom was described in the harmonic approximation. Secondly, the scale factor, extinction parameter and κ', κ'', P_v and P_{lm} were refined with all reflections. The multipole parameters of the K atom were small and statistically insignificant for the VCIP data and their values were taken to be zero. Finally, the displacement parameters were refined over the high-angle region and multipole parameters were then refined over all reflections. They were stable to within 0.2 of their e.s.d. The largest correlation was observed between U^{11}(F) and d_{1111}(F) parameters for 4C data and between scale factors and U^{11}(Ni) for VCIP data. The absolute values of the correlation coefficients were 0.91 and 0.92, respectively. The statistical correctness of the final results was checked using the Abrahams & Keve (1971) test.†

The lowest extinction factor was observed for the 002 reflection in both experiments: $y_{min} = 0.807$ (4C) and 0.812 (VCIP; $I_{obs} = y_{min}I_{kin}$, where I_{obs} and I_{kin} are the observed intensity and its kinematic value, respectively).

In order to check the physical significance of the displacement parameters obtained, we calculated the atomic probability density functions, which are the Fourier transforms of the anharmonic temperature factors (the corresponding maps are deposited†). These functions are meaningful (positive) in all space and only slightly deviate from harmonic ones.

Comparison of the model VCIP and 4C structure factors is presented in Fig. 1. Final figures of merits as well as the multipole and displacement atomic parameters derived are listed in Table 2.

Table 2. *Harmonic and anharmonic displacement and multipole parameters of $KNiF_3$: four-circle diffractometer results are in the first line and imaging plate ones are in the second line*

	K	Ni	F
U^{11}	0.01266 (3)	0.00532 (1)	0.00569 (6)
	0.01274 (5)	0.00512 (3)	0.00615 (20)
U^{22}	U^{11}	U^{11}	0.01549 (5)
	U^{11}	U^{11}	0.01537 (13)
$d_{1111} \times 10^4$	–	−0.00029 (17)	−0.00079 (38)
	–	−0.0014 (5)	−0.0008 (12)
$d_{1122} \times 10^4$	–	0.00072 (36)	−0.0010 (14)
	–	0.00013 (96)	−0.000 (4)
$d_{-2222} \times 10^4$	–	d_{1111}	∼0.00016 (98)
	–	d_{1111}	−0.0022 (31)
$d_{2233} \times 10^4$	–	d_{1122}	−0.0019 (14)
	–	d_{1122}	−0.0006 (39)
n	4, 4, 6, 8	4, 4, 6, 8	2, 2, 3, 4
	4, 4, 6, 8	4, 4, 6, 8	2, 2, 3, 4
κ'	1.0	0.993 (3)	0.977 (1)
	1.0	0.979 (16)	0.975 (6)
$\xi\kappa''$	4.6 (10)	10.2 (2)	3.5 (3)
	6.0	10.0 (6)	6.4 (2.8)
P_v	0	9.71 (4)	7.419 (14)
	0	9.77 (6)	7.42 (2)
P_{20}	–	–	−0.014 (12)
	–	–	−0.005 (26)
P_{40}	0.06 (3)	−0.241 (10)	0.111 (17)
	0	−0.30 (3)	0.046 (39)
P_{44+}	0.04	−0.179	0.065 (15)
	0	−0.22	0.053(38)
$R(F)$, $wR(F)$,	0.0038, 0.0036		
	0.0073, 0.0106		
$R(\|F\|^2)$, $wR(\|F\|^2)$	0.0047, 0.0072		
	0.0115, 0.0212		
Goodness of fit (S)	1.22		
	1.15		

3.2. *Atomic orbital analysis*

The refinement with atomic orbitals (AO) was also performed. Anharmonicity of the atomic displacements up to tensors of fourth rank in the crystal field approximation: the overlap between Ni and F atoms was described using a method based on Boltzmann statistics (Dawson *et al.*, 1967; Tanaka & Marumo, 1983). The valence AO for eight 3*d* electrons of the Ni atom in the O_h crystal field were approximated as a linear combination of five real basis functions, φ_j, while 2*s* and $2p_x$, $2p_y$ and $2p_z$ orbitals were assumed to be valence atomic orbitals for the F atom and 4*s* for the K atom. No hybridized orbital model was assumed for the F atom. Therefore, the ED is approximated as the sum of the atomic contributions in the form

$$\rho(\mathbf{r}) = \rho_{core}(r) + \textstyle\sum_i P_i \Sigma\Sigma c_{ij}^* c_{ik} \varphi_j^*(\kappa_i r)\varphi_k(\kappa_i r),$$

which corresponds to the orbital minimal basis set pseudo-atomic approximation. The coefficients c_{ij} are

† Supplementary data for this paper are available from the IUCr electronic archives (Reference: AV0018). Services for accessing these data are described at the back of the journal.

constants owing to the high symmetry of the Ni atom: the corresponding relationships between c_{ij} coefficients of d electrons are tabulated by Tanaka (1988). Populations of the AO and 'scale' parameters κ_i for each AO not for the ED were included in the electron density model together with the scale factor, harmonic and anharmonic displacement parameters, and extinction according to Becker & Coppens (1974). They were found in the iterative way using the program *QNTAO* programmed by one of us (KT). The electroneutrality

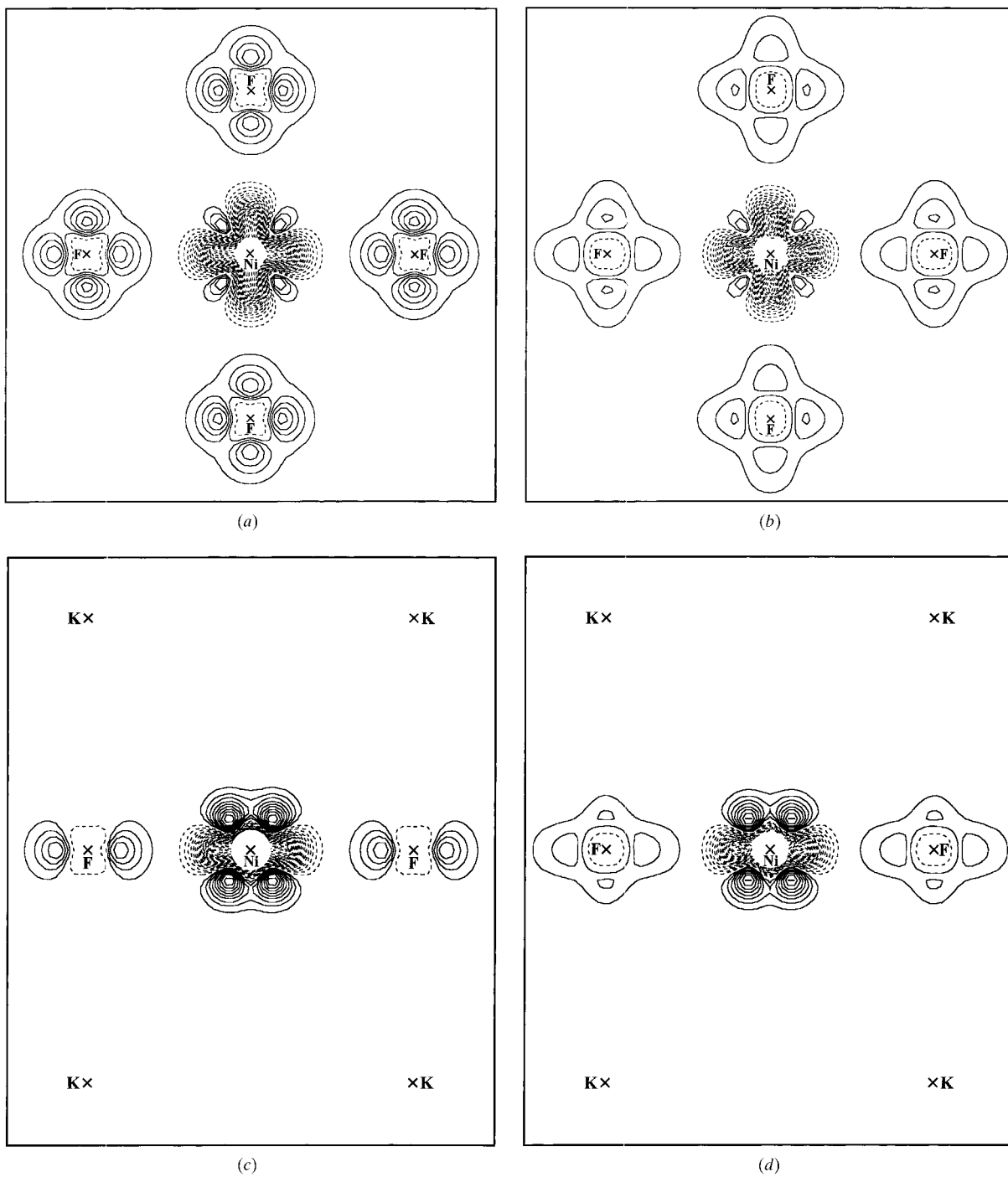

Fig. 2. Model static deformation electron density maps in the (100) and (110) planes of $KNiF_3$: (*a*) VCIP, (100) plane; (*b*) 4C, (100) plane; (*c*) VCIP, (110) plane; 4C, (110) plane. Contour intervals are 0.1 e $Å^{-3}$.

Table 3. *Orbital electron populations, P, and orbital 'scale' parameters, k, of atoms in $KNiF_3$ obtained from different experiments*

	4C	VCIP
K 4*s*: *P*	0.11 (2)	0.41 (3)
k	1.0	1.0
Ni 3*d*: *P* (e_g)	1.94 (4)	1.8 (1)
k (e_g)	0.98 (2)	1.08 (8)
P (t_{2g})	5.65 (2)	5.84 (7)
k (t_{2g})	1.017 (8)	0.99 (3)
Ni 4*s*: *P*	2.00 (9)	1.1 (8)
k	1.0	1.0 (2)
F 2*s*: *P*	2.0	2.0
k	1.0	1.0
F 2*p*: $P(p_x)$	1.842 (9)	2.00 (4)
$k(p_x)$	0.915 (5)	0.86 (1)
$P(p_y) = P(p_z)$	1.794 (7)	1.80 (3)
$k(p_y) = k(p_z)$	0.98(1)	0.99(3)
R	0.0036	0.0079
wR	0.0037	0.0115
S	0.99	1.04
Electron configuration		
Orbital refinement	$K^{+0.89}Ni^{+0.41}F_3^{-0.43}$	$K^{+0.59}Ni^{+1.26}F_3^{-0.6}$
Multipole refinement	$K^{+1}Ni^{+0.285}F_3^{-0.427}$	$K^{+1}Ni^{+0.242}F_3^{-0.413}$

condition was kept during the refinement. The p_x orbital of the F atom was directed along the Ni—F bond, while the populations of p_y and p_z AO were constrained to be the same. The electron populations found are given in Table 3 (the atomic displacement parameters are deposited).

To compare the 3*d*-atomic electron populations for the Ni atom with those recalculated from multipole population parameters, the approach of Holladay *et al.* (1983) was used. They derived the expressions relating both types of populations. The 3*d* AO populations of the Ni atom determined from the multipole parameters using these relations for both experiments are: $P(e_g)$ = 2.43 (3), $P(t_{2g})$ = 5.34 (6) for the 4C experiment and $P(e_g)$ = 2.29 (11), $P(t_{2g})$ = 5.53 (15) for the VCIP one. The electron configurations of the Ni atom presented in Table 3 were obtained after separation of the 4*s* and 3*d* parts of the atomic electron density: the neutral atom ratio of 3*d*:4*s* populations was estimated as 0.8:0.2.

4. Deformation electron density and topological analysis

The multipole parameters obtained for both experiments were used to calculate the static model electron deformation density, $\Delta\rho$, characterizing the redistribution of electrons when spherical atoms form the crystal. The program *SALLY* (Hansen, 1990) was used. These maps in the (100) and (110) planes of the $KNiF_3$ unit cell, containing all interatomic vectors, are shown in Fig. 2.

The topological analysis of the ED of $KNiF_3$ was performed using the *XPRO*98 program (Ivanov *et al.*, 1997). Laplacian maps of the ED calculated from the multipole parameters derived from the experimental structure factors for both experiments are presented in Fig. 3. We have also found all the critical points in the ED of $KNiF_3$ and calculated the curvatures of the ED,

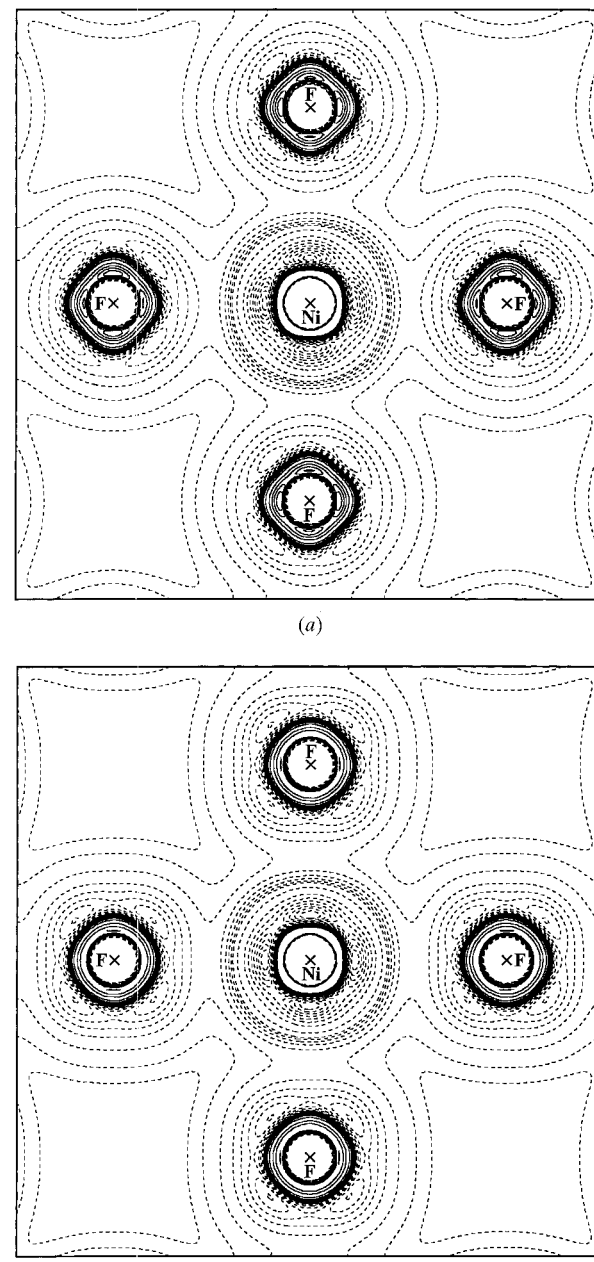

Fig. 3. Maps of the Laplacian of the electron density calculated from the multipole parameters in the (100) plane of $KNiF_3$: (*a*) VCIP; (*b*) 4C. Positive contours are dashed, negative ones are solid. Contour intervals are 1 e Å^{-5} for $-2 < \nabla^2\rho < +2$ e Å^{-5}, 5 e Å^{-5} for $-30 < \nabla^2\rho < -2$ e Å^{-5} and $+2 < \nabla^2\rho < +30$ e Å^{-5}, 50 e Å^{-5} for other values. Contours with $\nabla^2\rho < -500$ e Å^{-5} and $\nabla^2\rho > 500$ e Å^{-5} are omitted.

λ_i, in these points. These characteristics are listed in Table 4.

5. Electrostatic potential maps

The distributions of the electrostatic potential were calculated with multipole parameters using the program *XPRO*98 (Ivanov *et al.*, 1997). The average unit-cell potential calculated according to Becker & Coppens (1990) was taken as zero to define the electrostatic potential scale. These values are 0.60 (VCIP) and 0.59 e $Å^{-1}$ (4C). Maps of the electrostatic potential in the (100) plane of $KNiF_3$ are presented in Fig. 4.

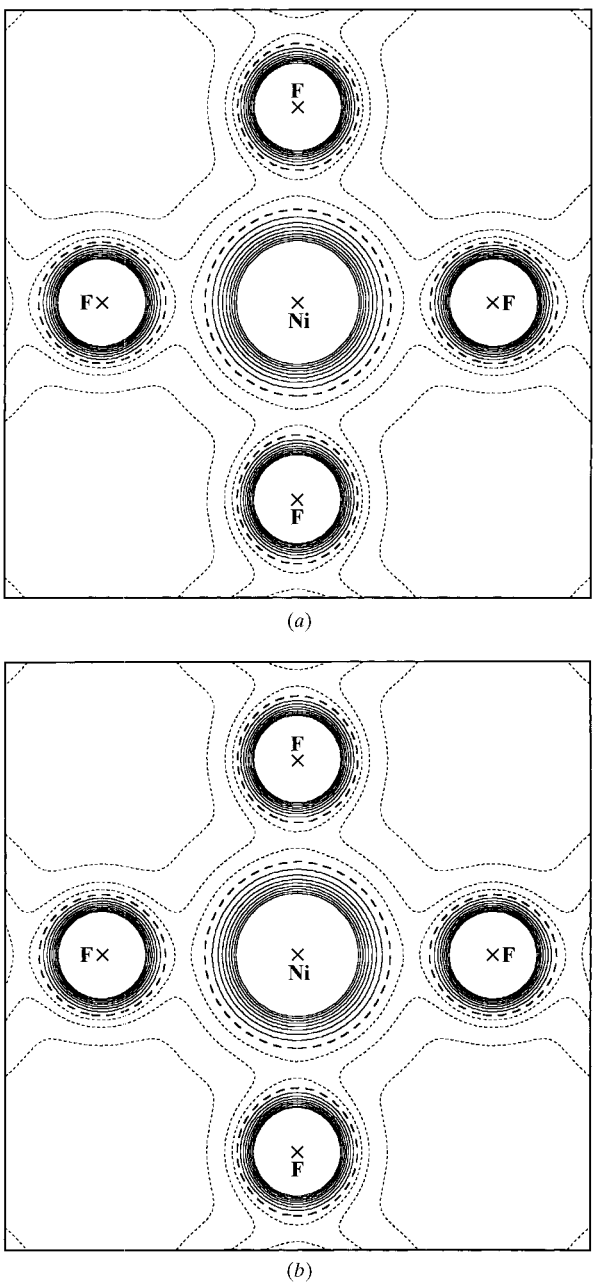

Fig. 4. Maps of the electrostatic potential in the (100) plane of $KNiF_3$: (*a*) VCIP and (*b*) 4C. Contour intervals are 0.2 e $Å^{-1}$. Positive contours are solid.

6. Discussion

6.1. *Comparison of the VCIP and 4C results*

The plot in Fig. 1 demonstrates reasonable agreement between structure factors obtained from the VCIP and 4C experimental data with the same multipole model. The biggest relative deviation of 1.55% is found for the 014 reflection, while the *R* factor between the two sets of structure factors is only 0.23%.

A maximal difference of 8% (or ~2 e.s.d.s) in the harmonic atomic displacement parameters is observed for the U^{11} parameter of the F atom (Table 2). Agreement between the anharmonic parameters is not as good, however, the signs of all the parameters are the same. Both sets of displacement parameters result in physically meaningful atomic probability density functions, which correspond to well defined single-well one-particle potentials.

Agreement of the multipole VCIP and 4C parameters is quite satisfactory: deviation within 1 e.s.d. occurs, excluding the P_{40} parameters of all atoms, for which it is within 2 e.s.d.s (Table 2). As a result, the deformation ED maps are similar. The VCIP peaks corresponding to the electron distribution around F atoms are, however, higher at ~0.2 e $Å^{-3}$.

Orbital populations obtained from the 4C data are similar to each other. For the VCIP data the agreement was not as good for the populations of the 4*s* orbitals of K and Ni, which are difficult to determine in reciprocal space. This is probably due to the less accurate determination of the low-angle reflections in the latter method.

We can outline a few reasons for the discrepancies mentioned. First, there are some errors in the determination of the Bragg peak position in any imaging plate method resulting from uncertainty in the determination of the orientation matrix (Tanaka *et al.*, 1999). Second, it is difficult to remove the two-dimensional 'tails' of the Bragg peak uniformly for all reflections in the VCIP method. This procedure should provide the net intensity with an accuracy comparable to that for the four-circle geometry. We tried to reach this accuracy by orienting the elliptical integration area along the direction of increasing $\sin\theta/\lambda$. Third, we discovered a noticeable extra intensity in some pixels after scanning the imaging plate. This is evidence that some random errors with an unknown distribution law occur in the imaging plate digitizing procedure.

At the same time, the VCIP and 4C Laplacians of the ED and the electrostatic potentials in interatomic space

Table 4. *Characteristics of the critical points in the $KNiF_3$ four-circle diffractometer results are presented in the first line and vacuum-camera-imaging plate ones are given in the second line*

Critical point position	X	Y	Z	$\rho(\mathbf{r}_{cp})$ (e Å^{-3})	$\nabla^2\rho(\mathbf{r}_{cp})$ (e Å^{-5})	λ_1 (e Å^{-5})	λ_2 (e Å^{-5})	λ_3 (e Å^{-5})	Type of critical point
$(x,0,0)$	0.2435	0	0	0.50 (2)	7.08 (19)	−2.45	−2.45	11.98	(3,−1)
	0.2436	0	0	0.45 (3)	8.01 (21)	−1.66	−1.66	11.33	
$(\frac{1}{2}, x,x)$	0.5	0.2395	0.2395	0.07 (1)	1.41 (4)	−0.26	−0.08	1.75	(3,−1)
	0.5	0.2393	0.2393	0.07 (1)	1.37 (6)	−0.23	−0.18	1.78	
(x,y,y)	0.139	0.352	0.352	0.04 (1)	0.60 (2)	−0.06	0.26	0.40	(3,+1)
	0.2394	0.2808	0.2808	0.05 (1)	0.63 (2)	−0.02	0.08	0.57	
$(0,\frac{1}{2},\frac{1}{2})$	0	0.5	0.5	0.02 (1)	0.28 (2)	0.08	0.08	0.12	(3,+3)
	0	0.5	0.5	0.02 (1)	0.21 (2)	0.06	0.06	0.09	
(x,x,x)	0.2666	0.2666	0.2666	0.04 (1)	0.59 (2)	0.03	0.03	0.53	(3,+3)
	0.2661	0.2661	0.2661	0.05 (1)	0.61 (2)	0.02	0.02	0.57	

(Figs. 3 and 4) are in good semi-quantitative agreement. Owing to an integral dependence on the charge density, the weaker potential depends on the local distortions of the ED. In contrast, the Laplacian map is a very sensitive measure of the ED: it shows that electron densities obtained with different diffraction techniques are indeed similar.

6.2. *Chemical bond and electrostatic potential in $KNiF_3$*

In spite of the existing problems mentioned, all deformation ED maps and topological characteristics of the ED exhibit a highly polar Ni—F bond and almost purely ionic K—F bond. The same conclusion results from the difference ED maps calculated for bulk $KNiF_3$ by Ricart *et al.* (1995) on the basis of the *ab initio* periodic Hartree–Fock method. It should be noted that our model deformation ED maps exhibit qualitatively the same patterns as the Fourier (dynamic) deformation ED calculated by Kijima *et al.* (1983) and Maslen & Spadaccini (1989). However, the noise level on the model maps is significantly lower.

The ED maps and qualitative characteristics given in Tables 2 and 3 show that the e_g-AO of the Ni atom, involved in σ bonds with F atoms, are depopulated in comparison to the spherical-atom case $(t_{2g})^{4.8}(e_g)^{3.2}$, while population of the t_{2g}-AO is slightly less than 6.

The electrostatic potential distribution in $KNiF_3$ has a 'muffin-tin' nature: it is slightly disturbed around Ni and F atoms by neighboring atoms (Fig. 4) and practically spherical around the K atom (picture not shown here). Inspection of such maps can help in the choice of approximation for the potential in the energy band calculations.

In conclusion, we have demonstrated that the vacuum-camera-imaging plate method combined with a rotating anode X-ray source is capable of providing accurate diffraction information, which is necessary for solid state physics and chemistry.

The support of this work by the Japanese Ministry of Education, Science, Sports and Culture (grant No. 09045034) is gratefully acknowledged.

References

Abrahams, S. C. & Keve, E. T. (1971). *Acta Cryst.* A**27**, 157–165.
Abramov, Yu. A., Tsirelson, V. G., Zavodnik, V. E., Ivanov, S. A. & Brown, I. D. (1995). *Acta Cryst.* B**51**, 942–951.
Becker, P. J. & Coppens, P. (1974). *Acta Cryst.* A**30**, 129–147.
Becker, P. J. & Coppens, P. (1990). *Acta Cryst.* A**46**, 254–258.
Bolotovsky, R., Darovsky, A., Kezerazhvili, V. & Coppens, P. (1995). *J. Appl.Cryst.* **28**, 86–95.
Buttner, R. H. & Maslen, T. (1988). *Acta Cryst.* C**44**, 1707–1709.
Dawson, B., Hurley, A. C. & Maslen, V. W. (1967). *Proc. R. Soc. London. Ser. A*, **298**, 255–263.
Graafsma, H., Svensson, S. O. & Kvick, Å. (1997). *J. Appl. Cryst.* **30**, 957–962.
Hansen, N. (1990). *SALLY. Program for Calculating Static Deformation or Valence Densities.* MS DOS version. LCM3B, Faculté des Sciences, Université Henri Poincaré, Nancy I, France.
Hansen, N. & Coppens, P. (1978). *Acta Cryst.* A**34**, 909–921.
Hellwege K.-H. (1979). Editor. *Landolt-Börnstein. Numerical Data and Functional Relationships in Science and Technology.* New Series. Group III, Version 11. Berlin: Springer-Verlag.
Holladay, A., Leung, P. & Coppens, P. (1983). *Acta Cryst.* A**39**, 377–387.
Ivanov, Yu., Abramov, Yu. & Tsirelson, V. (1997). National Conference on Application of the X-ray, Neutrons and Electrons for Study of Materials. Abstracts. Moscow, Dubna, p. 599.
Kijima, N., Tanaka, K. & Marumo, F. (1981). *Acta Cryst.* B**37**, 545–548.
Kijima, N., Tanaka, K. & Marumo, F. (1983). *Acta Cryst.* B**39**, 561–564.
Maslen,T. & Spadaccini, N. (1989). *Acta Cryst.* B**45**, 45–52.
Martin, A. & Pinkerton, A. A. (1998). *Acta Cryst.* B**54**, 471–477.
Miyata, N., Tanaka, K. & Marumo, F. (1983). *Acta Cryst.* B**39**, 557–561.
Otwinowski, Z. & Minor, W. (1997). *Methods Enzymol. A*, **276**, 307–326.
Protas, J. (1995). *MOLDOS*96/*MOLLY IBM PC-DOS*. Updated version (private communication).
Ricart, R., Dovesi, R., Roetti, C. & Saunders, V. R. (1995). *Phys. Rev. B*, **52**, 2381–2389.
Tanaka, K. (1988). *Acta Cryst.* A**44**, 1002–1008.

Tanaka, K., Kumazawa, S., Tsubokawa, M., Maruno, S. & Shirotani, I. (1994). *Acta Cryst.* A**50**, 246–252.
Tanaka, K. & Marumo, F. (1983). *Acta Cryst.* A**39**, 631–641.
Tanaka, K., Zhurova, E. A., Zhurov, V. V. & Kitamura, S. (1999). *J. Appl. Cryst.* To be published.
Tsarkov, A. G. & Tsirelson, V. G. (1991). *Phys. Status Solidi B*, **167**, 417–428.
Tsirelson, V. G. & Ozerov, R. P. (1996). *Electron Density and Bonding in Crystals.* IOP: Bristol and Philadelphia.
Zhurov, V. V. (1998). Unpublished work.
Zhurova, E. A., Zavodnik, V. E. & Tsirelson, V. G. (1995). *Crystallogr. Rep.* **40**, 816–823.
Zhurova, E. A., Zhurov, V. V. & Tanaka, K. (1999). *Acta Cryst.* B**55**, 917–922.